Article

Effect of Internal Donors on Raman and IR Spectroscopic Fingerprints of $MgCl_2/TiCl_4$ Nanoclusters Determined by Machine Learning and DFT

Maddalena D'Amore [1,*] 0000-0002-4248-8767, Toshiaki Taniike [2,] 0000-0002-4870-837X, Minoru Terano[2,] 0000-0003-3135-4744, and Anna Maria Ferrari [1,*] 0000-0003-1465-2774

1 Dipartimento di Chimica, Università di Torino, Via P. Giuria 5, 10125 Torino, Italy
2 Graduate School of Advanced Science and Technology, Japan Advanced Institute of Science and Technology, 1-1 Asahidai, Nomi, Ishikawa, 923-1292, Japan
* Corresponding author: maddalena.damore@unito.it (M.D.), anna.ferrari@unito.it (A.M.F.)

Abstract: To go deep inside the origin of Ziegler-Natta catalysis we need to fully understand the structure and properties of $MgCl_2/TiCl_4$/ID nanoclusters. In this work $MgCl_2/TiCl_4$ nanoplatelets derived by machine learning and DFT calculations have been used to model the interaction with ethyl-benzoate EB (as internal donor) with available exposed sites of binary $Ti_xCl_y/MgCl_2$ systems. The influence of vicinal Ti_2Cl_8 and coadsorbed $TiCl_4$ on energetic, structural and spectroscopic behaviour of EB has been considered. The adsorption of homogeneous-like $TiCl_4$EB and $TiCl_4(EB)_2$ at the various surface sites have been also simulated. Moving in the framework of Density Functional theory, we adopted B3LYP-D2 and M06 functionals. The adducts have been characterized by computing IR and Raman spectra that have been found to provide specific fingerprints useful to identify surface species; IR spectra have been successfully compared to available experimental data.

Keywords: polymerization catalysis, machine learning, nanoclusters, DFT, Raman spectrum, IR spectrum, Lewis bases

1. Introduction

In real heterogenous catalysts the complexity of the sytem is crucial in determing activity, selectivity and life-time, that represent the main parameters defining the performance of the catalyst; hence togheter with active species, dopants, promoters or modifiers need to be carefully chosen and their role fully understood. With regard to $MgCl_2$ supported Ziegler Natta catalysts (ZNC) for olefin polymerization, the electron donors (Lewis base molecules) have been providing that supporting activity since 1960s with significant increase of both catalyst productivity and stereospecificity. [1–4]

This very diffuse practice has been continously improved during last decades by industry mostly in a trial and error process.

The coadsorbtion of electron donors (generally bidentate organic molecules like diesters, diethers, and dialkoxysilanes) determine the local environment of the transition metal, behaving as ancillary ligand(s) in molecular catalysts able to enhance their regio- and enantioselectivity at the propene insertion in a defective context. They also determine the molecular weight distribution of the polymer, the distribution of active sites, the morphology of the catalyst [1,5–22] and the properties of the produced polymers. The industrial research in the last decade was devoted to the optimization of new couples internal donor/external donor (ID, ED) [21,22] because generally pairs of electron donors are used. [6,9,23,24]

Both experimental [25] and computational [26–32] research has been performed to get insights in the structure of ZNC at the atomic level, with main attention to the place and ways of binding of the ID, ED and their effects on the structure of the active sites.

Preprints (www.preprints.org) | NOT PEER-REVIEWED | Posted: 28 December 2021 doi:10.20944/preprints202112.0450.v1

Several contrasting hypotheses have been formulated about the role of the IDs. Some researchers claimed that the ID coordinates to a vacancy of the titanium centers, thus forming new active and stereo-specific sites;[33–36] it is also supported by the formation of homogeneous complexes between $TiCl_4$ and many Lewis base molecules. The other opposite hypothesis recall the historical one: the ID only interacts with the $MgCl_2$ support, indirectly determining the place and the distribution of the $TiCl_4$ moieties on the $MgCl_2$ surfaces and preventing the formation of aspecific sites.[33–40] Nowadays the most trusted and accepted hypothesis for ID, is the one known as the "coadsorption model": ID would coordinate to the $MgCl_2$ surfaces close to the titanium active sites, thus influencing their steric and electronic properties with no direct bonding. [22,27,28] We can assume a total consensus of scientific community on the nanostructured and disordered nature of the active δ form of $MgCl_2$ exposing surfaces and defective sites to adsorption of both $TiCl_4$ and internal donors to form Ziegler-Natta precatalyst. The hypothesis supported by experimental investigation, mostly by TEM microscopy, encountered a lot of limits in characterization due to these nanosize and disordered features, heterogeneity of sites, dilution of the active centres, air sensitivity. Theoretical and computational chemistry provided crucial insights in δ-$MgCl_2$, made feasible the modelling of each component and the analysis of different catalytic sites.[41–43]

Molecular mechanics investigation identified the (110) and the (104) lateral surfaces as the surfaces for the adsorption of monomeric $TiCl_4$ and stereo-selective dimeric Ti_2Cl_8 species, respectively.[44] However, togheter with some experimental inconsistencies, DFT studies have definitely set aside those models, after puzzling DFT predictions of adsorption energies of Ti_x Cl_y species on regular $MgCl_2$ surfaces and thanks to more recent reliable descriptions of the morphology of the δ-$MgCl_2$ particles. [45–53] Theoretical calculations on $MgCl_2$ bulk and surface structure exploiting periodic Density Functional Theory approaches including London interactions pointed out that $MgCl_2$ crystals in the absence of adsorbates mainly expose the (104) or other pentacoordinated surfaces, whereas the picture drastically changes in the presence of adsorbates (i.e. electron donors); in fact, regular $MgCl_2$ crystals expose the (110) surfaces at a relatively large extent when they grow in the presence of Lewis bases (small molecules such as methanol, ethanol, and dimethyl ether) or in presence of alkoxy silanes employed as external donors. [32,54] Thanks to Bravais' law it was possible to identify the most stable surfaces in terms of (surface) Gibbs Free Energy: (107), (012), (101), (015) and (110) ones. [55] The combination of a careful structural analysis of the supporting δ-$MgCl_2$ nanocrystals by synchrotron X-ray total scattering [42] with the definition of Wulff's polyhedron of $MgCl_2$ crystallites suggested that ball-milling of naked $MgCl_2$ produces a larger total surface area and modifies the relative extension of the surfaces,too. That would increase the stability of the lateral surfaces exposing strongly acidic tetracoordinated Mg^{2+} sites (i.e., the (110), (012) and (015) ones) at the expenses of the basal (001) one. The polar plot identifyed the presence of possible defective edges involving the (110) surface.[43] Inelastic Neutron Scattering (INS) spectroscopy,[56] able to sample all the first Brillouin zone (FBZ) and thus predicting the dynamical behaviour of materials, proved to be a powerful method to understand nano-sized systems and measure the degree of disorder of δ-$MgCl_2$ in terms of both translational and rotational contribution. A step forward to determine the morphology of platelets with dimensions comparable to those of primary particles, typically adopted in industrial catalysis (2-3 nm), have been made by us thanks to the adoption of a genethic algorithm; the calculations have been performed both in presence and in absence of $TiCl_4$.[57] Differently than in the case of naked $MgCl_2$ where the evolutionary plots allowed us to identify structures where the majority of sites are pentacoordinated Mg^{2+} sites, in presence of $TiCl_4$ (in a ratio 50/3 $MgCl_2/TiCl_4$) couples of tetracoordinated sites are present after the reconstrution of nano-particles. That occurrence represents the topological requirement for the formation of octahedral Ti species that will start the catalytic process. That "motiv" confirms the presence of inter-surfaces edges as possible favorable place for stereo-selective active

Preprints (www.preprints.org) | NOT PEER-REVIEWED | Posted: 28 December 2021 doi:10.20944/preprints202112.0450.v1

sites as also reported in previous computational studies adopting traditional Density Functional methods. [31,43] FT-IR spectroscopy of probing carbon monoxide also was used to estimate the presence and the relative extention of $MgCl_2$ surfaces .[55,58] Very recently the vibrational Far-IR and Raman simulations have been carried out on large models of $MgCl_2$ nanoclusters identified through a non-empirical structure determination to discuss the effect of the binding of various precatalytic complexes Ti_xCl_y on IR and/or Raman features. IR features do not allow to clearly identify the presence of a certain adduct but in Raman a drastical change occurs after $TiCl_4$ adsorption. The spectroscopic features identified are specific of $TiCl_4$ adduct on 110-like tetracoordinated Mg^{2+} sites and different in shape and frequencies from those obtained in the case of the dimeric adduct on pentacoordinated sites. Hence Raman spectroscopy provides clear fingerprints to recognize each adduct on defective positions on nanoplatelet of Ziegler-Natta catalysts.

In this work, we make a step forward towards complexity and pass to ternary donor $MgCl_2/TiCl_4$ systems; we looked to different way of binding of ethyl benzoate (EB) in relation to available Mg^{2+} sites of attachment and respect to positions of Ti_xCl_y complexes, thus following the still open hypotheses on the mechanism that donors adopt for affecting polymerization catalysis. Differently than previous papers, mostly addressing perfect surfaces (or steps between them), we can here investigate ways of adsorption on defective positions on nanostructured support with sites formed after a reconstruction in presence of $TiCl_4$.

Starting from model nanoplatelets ($50MgCl_2$ and $50MgCl_2/3TiCl_4$) identified by non-empirical structure prediction based on the genetic algorithm and DFT, as reported in recent papers of us [57,59,60] different way of binding were proposed and analysed, vibrational and Raman simulations were carried out to identify wheter or not it is possible to identify clear fingerprints of many possible adducts donor/$TiCl_4$ on nano-shaped $MgCl_2$. The possible formation of homogeneous-like $TiCl_4EB$ and $TiCl_4EB_2$ species was also considered. In the present paper, for simplicity, we address the location of ethyl benzoate (EB) on $MgCl_2$ and $MgCl_2/TiCl_4$ precatalyst, even if EB is not so largely adopted in industrial process. For sure, the number of experimental works pointed towards EB [61–65] by far overcomes studies on any other electron donor, make it easy to compare results with the literature reports at least in IR case. On the possibility to distinguish between different complexes, the Raman response for sure appears more informative but, at this very moment, experimental data are still not available on these systems even if groups are working on this topic and we foresee a future comparison between simulated and experimental data. Although the present findings are limited to the case of EB, the same approach can be easily applied to industrially more relevant electron donors and we are also immediately going to rehiterate the analysis to ternary systems fully obtained by machine learning techniques that is nanoplatelet of $50MgCl_2$ reconstructed in presence of both $TiCl_4$ and IDs.

2. Computational Models and DFT Calculations Details

As support for the adsorption of EB we adopted models of $50MgCl_2$ and $50MgCl_2/3TiCl_4$ nanoplates, computed by employing non-empirical structure determination thanks to a software that combines global structure search, based on a genetic algorithm, and local geometry optimization by means of DFT[59,60]. The size of nanoclusters is about 3 nm in diameter, comparable with the experimental size of the catalyst primary particles (ca. 2.4-4.0 nm)[42]; at the meantime the ratio between $TiCl_4$ molecules and $MgCl_2$ units equal to 50/3 corresponds to 2.69 wt%, similar to Ti content in a typical Ziegler-Natta catalyst.[59,60,66,67] The DFT[68,69] calculations reported in this paper were mainly based on the B3LYP global hybrid functional,[70,71] as implemented in the CRYSTAL program.[72,73] London interactions strongly influence the description of these materials containing not only Ti_xCl_y species but also organic molecules; hence, accounting for long-range correlation, was mandatory. The semi-empirical DFT-D2 approach of Grimme

Preprints (www.preprints.org) | NOT PEER-REVIEWED | Posted: 28 December 2021 doi:10.20944/preprints202112.0450.v1

and co-workers [74,75] was adopted together with the hybrid B3LYP functional; it is well assessed that combined procedure may successfully describe surface interactions and adsorption process also including organic molecules.[76,77] Single point energy calculations were run with M06 functional [78]on B3LYPD-2 minima.

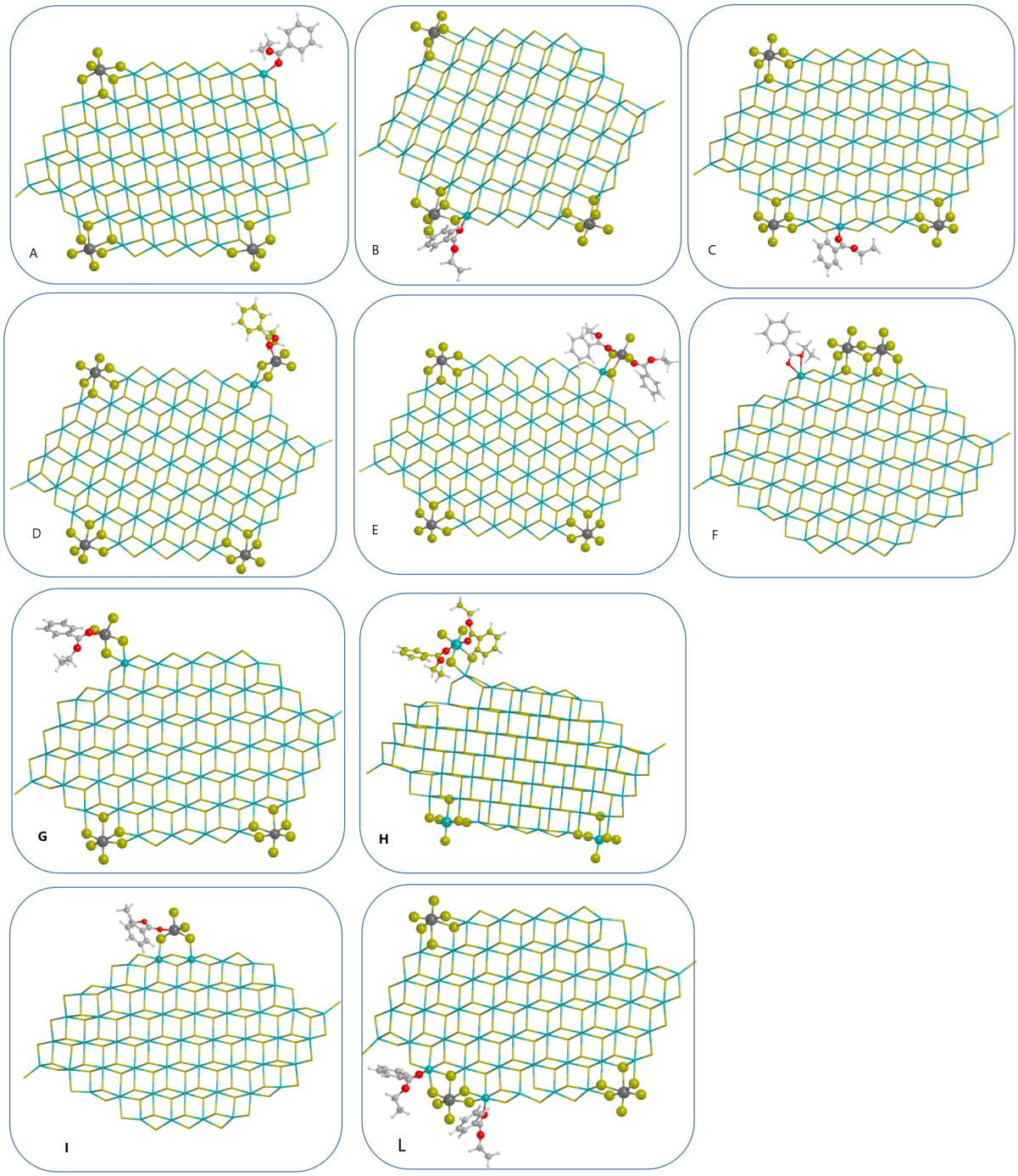

Figure 1. Coadsorption models of nanoplatelets (50$MgCl_2$/$TiCl_4$, see text for details) and EB with different way of binding (A-C); models of homogeneous-like $TiCl_4$ $(EB)_x$ (x = 1, 2) complexes on the same platelet (D, E, G, H) and models obtained after the coadsorption of EB and Ti_2Cl_8 on naked $MgCl_2$ nanoplatelet (F, I). Optimizations have been performed at B3LYP-D2/TZVP level. Chlorine, Magnesium and Titanium atoms are represented in green, yellow and dark grey, respectively. All generic atoms belonging to the nanoplatelet are represented as sticks, whereas atoms of $TiCl_4$ and EB molecules and Mg atoms involved in the adsorption process are reported as balls.

Preprints (www.preprints.org) | NOT PEER-REVIEWED | Posted: 28 December 2021 doi:10.20944/preprints202112.0450.v1

Split valence triple-zeta basis sets plus polarization (TZVP) of Gaussian type functions have been specifically customized and adopted for all the elements (Mg, Ti and Cl atoms).[51] Ahlrichs VTZ plus polarization quality [79] have been adopted for the adsorbed organic counterparts. The estimated energies have been corrected for Basis Set Superposition Error (BSSE). To inspect the molecular vibrational shifts of main modes involving CO group, O-C-O and $TiCl_4$ due to both the interaction with the support and the reciprocal interaction of organic and inorganic molecules, we run geometry optimizations followed by harmonic vibrational frequency calculations of the molecular adducts together with the corresponding IR and Raman intensities. Details about the computational set up and the calculations of the vibrational frequencies can be found in previuos works by us [57,80,81].

3. Results and Discussion

3.1. Models of ternary systems $MgCl_2/TiCl_4$/EB

The models of coadsorption of EB and $TiCl_4$ on nanoplatelet of $MgCl_2$ may be collected in three groups.

We built a first group of models (A, B, C, L in Figure 1) where the EB is added in different positions with respect to $TiCl_4$ aiming to investigate the effect of reciprocal perturbation on the vibrational response of both internal donor and precursor of active species. Here, due to the heterogeneity of sites, the adsorption of both $TiCl_4$ moieties (and its dimeric form Ti_2Cl_8) and EB on defective sites has been possible with many combinations of reciprocal positions donor/precatalytic species: edge-like for one between them, EB next to Ti moieties, EB far enough from Ti species to remain more or less unperturbed.

A second group (models D, E, G, H) accounts for the possibility of adsorption of homogeneous-like complexes, already present in reaction medium, to nanoclusters with different Ti/EB ratio, i.e. $TiCl_4$EB and $TiCl_4(EB)_2$ on various sites. Previous calculation on internal donor plus $TiCl_4$ adducts have been carried out by some of us on perfect surfaces at different degree of coverage, in that case we considered tetracoordinated Mg^{2+} ions of the type exposed on (110) surface [61] and (107) surfaces to adsorb in different way of binding EB on perfect surfaces.

A third group of models attains the Ti_2Cl_8EB complexes (F, I) on pentacoordinated Mg^{2+} sites because historically these type of adducts emulate those formed on (104)-like surfaces claimed to be able to bind Ti_2Cl_8, that was previously identified as the stereoselective active species for polypropylene.[38]. Although QM calculations proved that adsorption of Ti_2Cl_8 dimers on $MgCl_2$ surfaces is not feasible,[51] the presence of the donors might modify the energy of the adsorption process, giving a new chance for the adduct formation.

In the case of adducts EB/Ti_2Cl_8, after the adsorbtion on a penta-coordinated row of Mg^{2+} sites; the dimer breaks in an adsorbed $TiCl_4$EB complex and a $TiCl_4$ molecule physisorbed on the row, after the remotion of physisorbed $TiCl_4$ molecule, the $TiCl_4$EB adsorbed on cluster has been investigared further as Model I. Model F presents a molecule of EB bound to four-coordinated Mg^{2+} and adjacent to Ti_2Cl_8 dimer.

For most reasonable models, the IR and Raman vibrational frequencies have been calculated and reported in Figure 2 whereas the energetics is reported in Table I (in terms of total electron energy) together with some reaction energies.

3.2. IR and Raman response of EB/$TiCl_4$ on nanoplatelet

3.2.1. IR simulations

We first recap main IR feautures of EB and $MgCl_2/Ti_xCl_y$. The IR spectrum of EB is reported in panel a of Figure 1. The spectrum is overlooked by two intense peaks at 1766 and 1277 cm^{-1}; the band at 1766 cm^{-1} is assigned to ν(C=O) stretching mode, whereas that at 1277 cm^{-1}, coupled with the bands at 1130 and 1140 cm^{-1}, is due to a ν(C-O) stretching mode in the (C-O-C). Most of the other weak bands in the spectrum are related to C-H stretching (about 3000 cm^{-1}) or deformation modes of the phenyl ring and of the

Preprints (www.preprints.org) | NOT PEER-REVIEWED | Posted: 28 December 2021 doi:10.20944/preprints202112.0450.v1

ethyl group, (e.g., the weak bands at 1200 and 1098 cm^{-1} is associated with -CH bending of the phenyl ring whereas 1334, 1349 cm^{-1} modes are due to ring deformation and the very weak bands at 1403 and 1432 cm^{-1} are associated to the wagging of CH_3). It is very widely reported that the positions of the absorption bands ν(C-O) and ν(C-O-C) change upon EB complexation, whereas the others are much less sensitive. Due to the fact that we investigate a coadsorption with Ti_xCl_y, also the region 400-650 cm^{-1} has been here reported for the first time since our recent investigations on binary systems $TiCl_4$ /$MgCl_2$ revealed that the region cannot be neglected in IR spectra and even more in Raman analysis.

Concerning the IR response of $MgCl_2/TixCl_y$ nanoplatelets, it covers a region between 200 and 500 cm^{-1}[57]; altough the 200-400 cm^{-1} region refers to bulk modes, strongly dependent on the particle shape and size, the 400-500 cm^{-1} region contains fingerprints that can be easly correlated to surface sites and adorbed species: peaks at 429 and 445 cm^{-1} related to exposed tetracoordinated Mg^{2+} typical of 110 surfaces, a couple of bands at 465 and 485 cm^{-1} attributed to symmetric and antysimmetric stretching of Ti-Cl bonds in supported $TiCl_4$ and 458, 476 and 495 cm^{-1} bands for supported Ti_2Cl_8.

We considered now the adsorption of EB, according to the models sketched in Figure 1. IR spectra are reported in Figure 2, by considering separately the two vibrational regions 400-650 cm^{-1} and 1200-1750 cm^{-1} in order to better highlight the Ti_xCl_y and the EB response. Panels b, c and d of Figure 2 refer to model A-C that corresponds to EB coadsorption at almost isolated tetracoordinated and pentacoordinated Mg^{2+} (panels b and d) and EB coadsorbed at a pentacoordinated Mg^{2+} in proximity of a $TiCl_4$ surface specie of the precatalist (panel c). Panels e, and f of Figure 2 refer to models D-E of Figure 1. Panel g refers to model F. In Model D and F the $TiCl_4$/EB and $TiCl_4$/(EB)2 homogeneous-like complexes are loosely bound to the $MgCl_2$ surface through bridging chlorine atoms.

The main features of the spectra are:

- the ν(C=O) vibration that dominates the IR spectrum and is located at 1683, 1697 and 1695 cm^{-1} for models A-C, downshifted by 83, 69 and 71 cm^{-1} in reference to gas phase, respectively. Two very weak satellite bands are also osberved at 1638 and 1615 cm^{-1} that corresponds to C-C stretching modes of the phenyl ring. In the presence of a $TiCl_4$/EB adduct the C=O stretching mode undergoes a huge redshift to 1587 cm^{-1} (medium); it is further redshifted to 1556 cm^{-1} and coupled with a very weak band at 1585 cm^{-1} in the case of adduct E: they correspond to the antisymmetric and to the symmetric coupling of the two C=O stretchings;
- the ν(C-O) signal drops its intensity with respect to free EB and is splitted into three components at 1308, 1323, 1336; 1312, 1332,1348 and 1313, 1329, 1344 cm^{-1} for models A-C, respectively due to coupling with CH_2 twisting and phenyl H modes; however for model A the triplet of bands have comparable intensity, whereas for model B and C the band at higher wavenumber dominates in the triplet. A similar group of bands is observed for models D and E with the most intense peak located at 1362 cm^{-1};
- a new weak band appears at 1414,1418, 1417 cm^{-1} for models A-C, and at 1427 cm^{-1} for models D-E, is associated to the wagging of -CH_3 and therefore slightly perturbed by different EB binding mode; the band is weak but it can be clearly identified in the IR spectra;

Preprints (www.preprints.org) | NOT PEER-REVIEWED | Posted: 28 December 2021 doi:10.20944/preprints202112.0450.v1

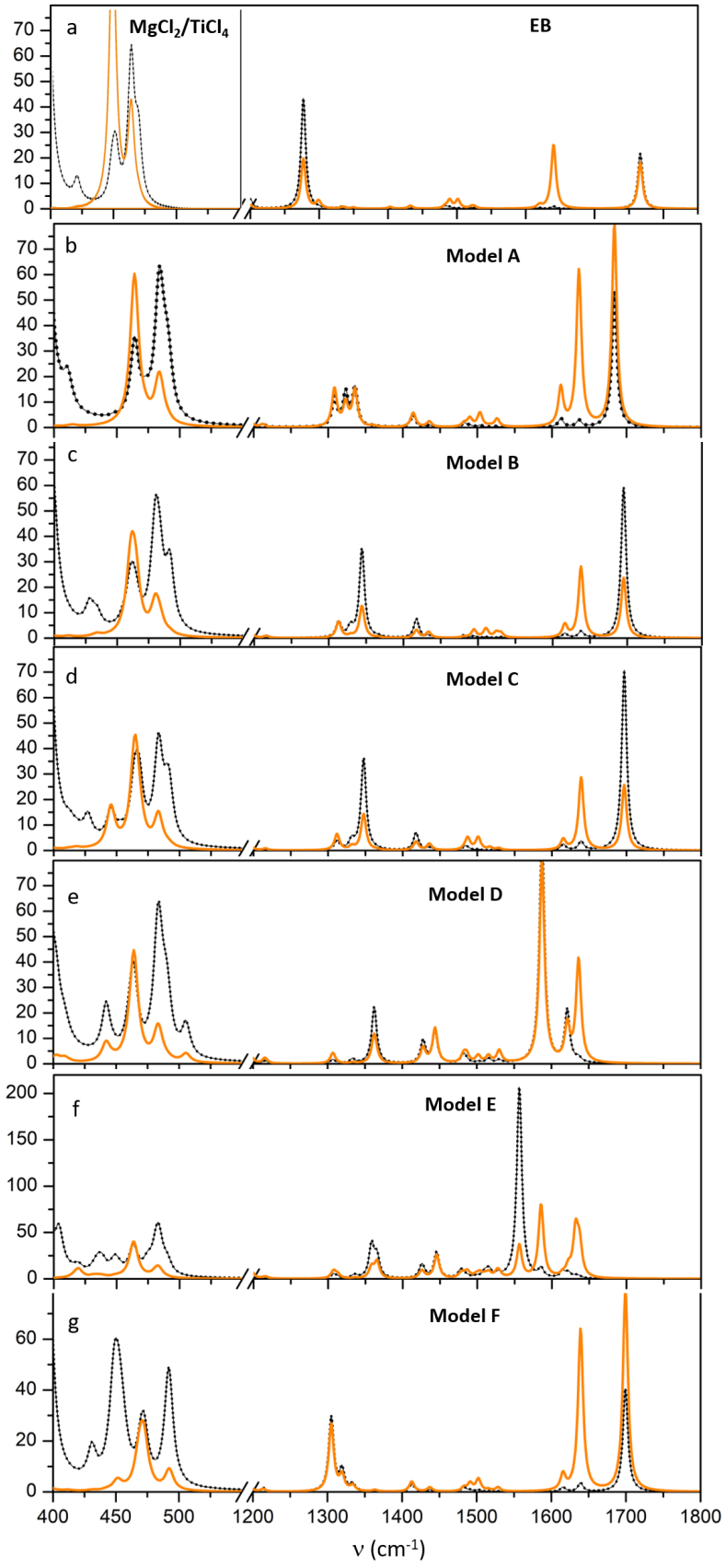

Figure 2. Simulated IR (black, dotted lines) and Raman spectra (orange, solid lines) at B3LYP-D2/TZVP for models proposed in Figure 1 in the spectral regions 400 - 550 cm^{-1} and 1200 - 1800 cm^{-1}. Intensity are in (Km/mol) and arbitrary units, respectively.

Preprints (www.preprints.org) | NOT PEER-REVIEWED | Posted: 28 December 2021 doi:10.20944/preprints202112.0450.v1

- the 400-500 cm^{-1} region. For systems A and B the Ti-Cl stretching mode at 465 and 485 cm^{-1} are only slightly perturbed by the presence of EB; for model C the coupling with EB mode causes the Ti-Cl symmetric stretching mode to split in components at 464, 465, 468 cm^{-1} and antisymmetric Ti-Cl stretching at 483, 484, also partially coupled with Mg-Cl modes of tetrahedral Mg^{2+} at 490 cm^{-1}. For models D-E two further bands, not visible in Raman, pop-up at 437 cm^{-1} and at 449 cm^{-1} due to bending modes of O-Ti-O and Ti-O-C, respectively. Weak bands at 588, 645 cm^{-1} assigned to Ti-O-C appear.

3.2.2. Raman characterization $MgCl_2/TiCl_4$/EB adducts

Let us consider first the EB molecule by itself in gas phase, see Fig.2 panel a. The main differences with respect to the IR counterpart are: i) the much higher intensity of the 1640 and 1620 cm^{-1} bands, due to C-C stretching of the phenyl ring; ii) a band falling at 1019 cm^{-1} related to phenyl ring deformations; iii) a significant increase in intensity for the triplet 1483, 1489, 1501 cm^{-1} due to modes involving the O-C-O group.
For EB supported adducts the main difference in the Raman spectra with respect to IR is the presence of the two intense bands at $\sim$ 1636 and 1612 cm^{-1} related to the C-C stretching of the phenyl ring that appear almost unperturbed in all the models, and the antisymmetric and symmetric coupling of the two C=O stretchings of model E that, at variance of IR, give rise to peaks of comparable intensity at 1556 and 1585 cm^{-1}, thus unambiguously probing the presence of $TiCl_4(EB)_2$.
All the other peaks are common in the IR and Raman spectra even if with different relative intensity.

3.3. Adsorption properties of adducts on $MgCl_2$ nanoplatelets

Adsorption energies of selected models are collected in Table 1. Models A, B, C, L represents different coadsorption possibilities for $TiCl_4$ molecules and EB molecules. In the case A, one EB molecule is bound to isolated T site and close to a row of pentacoordinated Mg^{2+} sites hence reproducing a sort of edge condition. Models B and C similarly reproduces different EB on a P site: the first is perturbed by the presence of $TiCl_4$ whereas the latter is almost unaffected by $TiCl_4$. In all three cases the adsorption energies are close each other (78-79 kJ/mol) with only a tiny larger energy in the adsorption to T site (A) but we can assume difference falls in the error bar. In model L the co-adsorption involve two EB molecules next to $TiCl_4$, the energy involved in the adsorption of a second molecule on an adjacent site to $TiCl_4$, as indicated in the reaction reported in Table I, is expected to be highly favored from an enthalpic point of view (ΔE=-121.9 kJ/mol). In case F, the perturbation comes from the dimer Ti_2Cl_8 on sites of P type; the adsorption energy predicted for EB in presence of Ti species strengthens the binding of EB up to -99.3 KJ/mol, in fact in this case a chelation through O(R) occurs resembling a diester mode coordination. The other models D, G, E, H, I attain the adsorption of complexes $TiCl_4EB_x$ (x=1,2), on defective T positions and only in the last case (I) on P position close to a couple of T Mg^{2+} sites. The mono-EB specie is weakly bound to T sites whereas the largest binding energies belong to the di-EB homogeneous-like adducts. A stronger interaction is predicted in the case G respect to D due to the presence of an adjacent most acidic T site. In the case G, the complex $TiCl_4EB$ is bound to one between a couple of adjacent tetracoordinated Mg^{2+} sites in a 110-like manner; that differs from the outcome of previous periodic 2D calculations where the structure $TiCl_4EB$/(110) evolves towards a new one with EB directly bound to support by carbonyl oxygen and at the meantime to a five coordinated $TiCl_4$ (Mg-O-Ti binding). This can be rationalized in terms of donor-donor interaction when periodic boundary conditions are assumed (even at low degree of coverage) and donor-adjacent layers of $MgCl_2$. In the models presented here bulky donors have larger degrees of freedom to keep a Mg-Ti-O binding. $TiCl_4$ is partially detached from surface and that leaves coordination vacancies around titanium where a further EB molecule can easily insert to get a significant gain in energy because

Preprints (www.preprints.org) | NOT PEER-REVIEWED | Posted: 28 December 2021 doi:10.20944/preprints202112.0450.v1

Ti keeps a six-fold coordination due to two EB molecules bonded through carboxyl oxygen; that is the case of models E and H. In model I the adsorption energy of $TiCl_4EB$ on P-type is close to case G, supporting the hypothesis that the presence of donor allows the binding of $TiCl_4$ on rows of 104-like Mg^{2+} sites contrary to an effective no binding of single $TiCl_4$ predicted in literature on 104 surfaces. For all the above-mentioned cases the adsorption energy has been computed by means of B3LYP-D2 method and in some selected cases, single points calculations have been carried out by employing the M06 functional as shown in Table 1.

In models close to truly nanosized structures, the clean break between the adsorption behaviour of T and P sites , emerging from a periodic approach, seems to become smoother; that can be due to the proximity of a few sites of the first type to the ones of the latter with consequent polarizing effect coming from the T sites on closer P ones. The adsorption energy reveals that the binding of EB is only tinily sensitive to the site of adsorption due to the frontier behaviour of sites. In particular, in the case of model B, where the proximity of $TiCl_4$ increases the polarizing ability of pentacoordinated Mg^{2+} (as we already found in probing cluster sites by CO[57]), the adsorption energy almost equal in model A and model B. In the case of model C the adsorption energy is only weakly affected due to the finite nature of support model and the fact that we are simply considering a monoester (for simplicity) with no strong ability to chelate the tetracoordinated sites present in type A models. In the case of homogeneous-like complexes, the complex with two EB molecules (model E) is by far more strongly bound to cluster, in fact in mono-EB case (models D, G), a large distortion occurs with respect to the geometry adopted from molecule of EB in the gas phase with a cost amounting to 34.5 kJ/mol. For model D, the significant difference with the results obtained for extended surfaces [61] is due to the fact that the minimum is unstable; it evolves towards a structure where EB is bound to an adjacent tetracoordinated site, in other words the $TiCl_4EB$ is bonded to $MgCl_2$ through the oxygen of the ester group.

Table 1. Energetics of adsorption of EB, $TiCl_4EB$ and $TiCl_4EB_2$ complexes for models reported in Fig.1 (energies in kJ/mol). All calculations were performed by adoption of B3LYP-D2 and M06 functionals and Ahlrichs VTZP basis set. In M06 case, single point energy calculations have been computed on geometries optimized at B3LYP-D2 level. All data are BSSE corrected.

Reaction	Model	ΔE(B3LYP-D2)	ΔE(M06)
$EB_{gas}+(MgCl_2TiCl_4)_{surf} \rightarrow (MgCl_2TiCl_4...EB)_{surf}$	A	-79.3	-81.6
"	B	-78.9	-80.9
"	C	-77.5	-79.5
$TiCl_4EB_{gas}+(MgCl_2TiCl_4)_{surf} \rightarrow (MgCl_2TiCl_4EB)_{surf}$	D	-66.3	-75.4
$TiCl_4EB_{2gas}+(MgCl_2TiCl_4)_{surf} \rightarrow (MgCl_2TiCl_4EB_2)_{surf}$	E	-181.2	-185.8
$EB_{gas}+(MgCl_2Ti_2Cl_8)_{surf} \rightarrow ((MgCl_2Ti_2Cl_8...EB)_{surf}$	F	-99.3	-96.0
$TiCl_4EB_{gas}+(MgCl_2TiCl_4)_{surf} \rightarrow (MgCl_2TiCl_4EB)_{surf}$	G	-79.3	-94.9
$TiCl_4EB_{2gas}+(MgCl_2TiCl_4)_{surf} \rightarrow (MgCl_2TiCl_4EB_2)_{surf}$	H	-172.1	-191.6
$TiCl_4EB_{gas}+(MgCl_2Ti_2Cl_8)_{surf} \rightarrow (MgCl_2TiCl_4EB)_{surf}$	I	-79.5	-95.3
$EB_{gas}+(MgCl_2TiCl_4...EB)_{surf} \rightarrow (MgCl_2TiCl_4...EB_2)_{surf}$	L	-121.9	-123.6
$(MgCl_2TiCl_4...EB)_{surf} \rightarrow (MgCl_2TiCl_4EB)_{surf}$	G	35.5	60.9
$(MgCl_2TiCl_4...EB_2)_{surf} \rightarrow (MgCl_2TiCl_4EB_2)_{surf}$	H	55.5	67.8

3.4. Discussion and Conclusions

EB is adsorbed at T and P isolated sites (models A and C) and at T and P sites adjacent to preadsorbed $TiCl_4$ and Ti_2Cl_8 (models B and F) giving rise to surface adducts of comparable stability ($\sim$ 80 kJ/mol, B3LYP-D2 and M06 results, Table 1). Physisorbed

Preprints (www.preprints.org) | NOT PEER-REVIEWED | Posted: 28 December 2021 doi:10.20944/preprints202112.0450.v1

EB on $TiCl_4$ and Ti_2Cl_8 cannot be identified since EB on Ti_2Cl_8 causes the fragmentation of the Ti cluster into $TiCl_4$/EB (model G) and physisorbed $TiCl_4$. The formation of the $MgCl_2$/EB adducts is monitored by the IR spectra.
Line a of Fig. 3 reports a convolution of IR spectra of the most relevant $MgCl_2$/EB surface structures in presence of $TiCl_4$ (sum of simulated intensities for models A, B, C and F). Inspection of the spectrum shows that the two main features are the ν(C=O) peak, sharp and narrow (its width is $\sim$ 12 cm^{-1}), centered at 1678 cm^{-1} and the ν(C-O-C) vibration that leads to a group of signals in the 1275-1350 cm^{-1} range; ν(C=O) peak appears to be sensitive to the coordination number of Mg^{+2}, but scarcely affected by the chemical environment of the surface cations, and similarly the characteristic shape of the ν(C-O) signal can unambiguously probe a simultaneous presence of tetra and pentacoordinated Mg^{+2} sites (compare panel d to panel f of Figure 2).
The homogeneous like $TiCl_4EB$ and $TiCl_4EB_2$ complexes can easily bind at the the Mg^{+2} sites of $MgCl_2$. However the only species present on P sites of the 104-like row is the $TiCl_4EB$ (model G); on T sites (i.e. 110-like sites) both $TiCl_4EB$ and $TiCl_4EB_2$ can be coordinated. The relative binding energies are quite similar for $TiCl_4EB$ adducts, $\Delta E \sim$ 70-80 kJ/mol (B3LYP-D2), but much larger for $TiCl_4EB_2$, $\Delta E \sim$ 170-180 kJ/mol (B3LYP-D2).
Convoluted IR spectrum of adsorbed $TiCl_4EB_x$ complexes (sum on spectra of models D and E) reported as line b of Figure 3, show that the $TiCl_4EB$ complex is associated with two signals centered at about 1620 cm^{-1} due to ring deformations coupled to C=O stretching whereas $TiCl_4/(EB)_2$ is unambiguously characterized by a band at 1556 cm^{-1}, due to carbonyl couples, that dominates the IR spectrum.

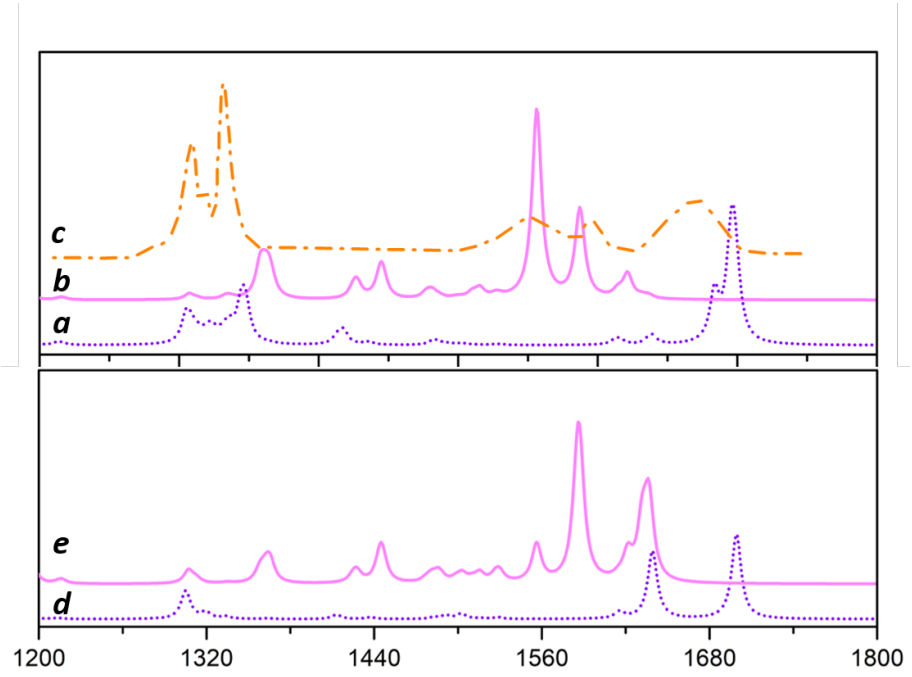

Figure 3. Sum of simulated IR intensity at B3LYP-D2/TZVP, for co-adsorption models A, B, C, F (line a) and for homogeneous-like adducts, models D, E, (line b). Experimental IR spectrum from Ref. [61] reported in the 1200-1350 and 1550-1800 cm^{-1} spectral range (line c). Sum of simulated Raman intensity at B3LYP-D2/TZVP, for co-adsorption models A, B, C, F (line d) and for homogeneous-like adducts, models D, E, (line e). The spectral region considered is 1200 - 1800 cm^{-1}, the intensities are in arbitrary units.

We can notice the excellent agreement between computed IR spectra of Figure 3a-b and the experimental one of $MgCl_2/EB/TiCl_4$ from Ref. [61] and reported in Figure 3b; the larger discrepancy can be found in the region of ν(C=O) (CO stretching) with a shift

that can be easily attributed to anharmonicity of the mode, neglected in the harmonic approximation we adopted. Concerning the Raman response, convoluted spectra are reported in Figure 3d-e. The high frequency region is dominated by two intense peaks at 1720 cm^{-1} due to ν(C=O) and at 1660 cm^{-1} associated to C-C stretching mode of the phenyl ring; the 1275-1350 cm^{-1} range shows a group of signals related to ν(C-O). Adsorbed $TiCl_4EB_{1,2}$ provide clear fingerprints in the Raman spectra: the couple of bands at 1660 (with a shoulder at 1642 cm^{-1}) and at 1606 cm^{-1} identifies the mono-EB adduct, whereas the presence of an additional peak at 1576 cm^{-1} reveals the presence of the di-EB adduct.

The formation of homogeneus like $TiCl_4EB_{1,2}$ at the $MgCl_2$ nanoplatelets is thus unumbiguosly probed by IR and Raman spectra. However we can wonder about the role, if any, of the $MgCl_2$ substrate in promoting the formation of those surface complexes. Starting from $MgCl_2$/EB, $TiCl_4$ can be bound on a couple of adjacent T sites even in the presence of preadsorbed EB at one of the T centers ($MgCl_2$/$TiCl_4$...EB, model B of Figure 1 and Table 1) with a binding energy of -91.6 kJ/mol, (the corresponding value on bare $MgCl_2$ is 69.0 kJ/mol). In the same way, starting from $MgCl_2$/$TiCl_4$, EB can absorb at the one of the T sites that binds $TiCl_4$ (again model B) with a coordination energy of -106.9 kJ/mol (M06). Despite sharing the same Mg^{+2} center, both $TiCl_4$ and EB are strongly bound to the substrate; thus a surface reaction starting from $MgCl_2$/$TiCl_4$...EB (Model B) and leading to $MgCl_2$/$TiCl_4$(EB) (model E) is energetically not favored by $\sim$ 61 kJ/mol, Table 1. We consider now a couple of EBs adsorbed on adjacent T sites; coordination of $TiCl_4$ involving the same T sites is again energetically favored by -103 kJ/mol: hence, coadsorption, first with one and then with two EBs progressively improves $TiCl_4$ coordination to $MgCl_2$. Similarly a second EB molecule succesfully coadsorbes on $MgCl_2$/$TiCl_4$...EB leading to Model L with an associated energy variation ΔE=-123.6 kJ/mol. Hence, EB and $TiCl_4$ act cooperatively and stabilize each other so that, the presence of a second coadsorbed EB further disfavors a spontaneous evolution to the homogeneous like $TiCl_4(EB)_2$ surface adduct (Model H) and the corresponding reaction is disadvantaged by 68 kJ/mol, Table 1. Indeed, it is experimentally known that $TiCl_4$/EB complexes dissociatively adsorb on $MgCl_2$.[82] The presence of donor allows the binding of $TiCl_4$ on rows of 104-like Mg^{2+} sites (model I) contrary to an effective no binding of single $TiCl_4$ predicted in literature on 104 surfaces.

Author Contributions: Conceptualization, T. Taniike and M. Terano; methodology, M. D'Amore; software, A.M. Ferrari and M. D'Amore for CRYSTAL code, T. Taniike and M. Terano for genethic algorithm; validation, A. M. Ferrari, M. D'Amore; investigation, M. D'Amore; resources, M. D'Amore; data curation, A.M. Ferrari; writing—original draft preparation, M. D'Amore; writing—review and editing, M. Terano, A. M. Ferrari, T. Taniike; visualization, M. D'Amore; supervision, M. Terano, A. M. Ferrari. All authors have read and agreed to the published version of the manuscript.

Acknowledgments: Authors benefitted from access to the HPC resources of CINECA, thanks to ISCRA C project: SEILIM HP10C0DEN5. Authors acknowledge: SCARF Scientific Computing Department, STFC Rutherford Appleton Laboratory for computer facilities. Dr. Svemir Rudic and Jonatan Roddom are kindly acknowledged for technical support.

Conflicts of Interest: Authors declare no conflict of interest

References

1. Chadwick, J.C. Advances in propene polymerization using MgCl2-supported catalysts. Fundamental aspects and the role of electron donors. *Macromol. Symp.* **2001**, *173*, 21–36.
2. Cecchin, G.; Morini, G.; Pelliconi, A. Polypropene product innovation by reactor granule technology. *Macromol. Symp.* **2001**, *173*, 195–210.
3. Busico, V. Giulio Natta and the development of stereoselective propene polymerization. *Adv. Polym. Sci.* **2013**, *257*, 37–58.
4. Albizzati, E.and Giannini, U.; Collina, G.; Noristi, L.; Resconi, L. *Catalysts and polymerizations. In Polypropylene Handbook*; Moore, E.P. J.; Hanser-Gardner Publications: Cincinnati, OH, (1996).
5. Taniike, T.; Terano, M. The use of donors to increase the isotacticity of polypropylene. *Adv. Polym. Sci.* **2013**, *257*, 81–97.

6. Busico, V.; Corradini, P.; De Martino, L.; Proto, A.; Savino, V.; Albizzati, E. Polymerization of propene in the presence of $MgCl_2$-supported Ziegler-Natta catalysts 1. The role of ethyl benzoate as "internal" and "external" base. *Makromol. Chem.* **1985**, *186*, 1279–1288.
7. Busico, V.; Chadwick, J.C.; Cipullo, R.; Ronca, S.; Talarico, G. Propene/ethene-[1-C-13] copolymerization as a tool for investigating catalyst regioselectivity. $MgCl_2$/internal donor/$TiCl_4$-external donor AlR_3 systems. *Macromolecules* **2004**, *37*, 7437–7443.
8. Soga, K.; Shiono, T.; Doi, Y. Influence of internal and external donors on activity and stereospecificity of Ziegler-Natta catalysts. *Makromol. Chem.* **1988**, *189*, 1531–1541.
9. Sacchi, M.C.; Tritto, I.; Shan, C.; Mendichi, R.; Noristi, L. Role of the pair of internal and external donors in $MgCl_2$-supported Ziegler-Natta catalysts. *Macromolecules* **1991**, *24*, 6823–6826.
10. Sacchi, M.C.; Forlini, F.; Tritto, I.; Mendichi, R.; Zannoni, G.; Noristi, L. Activation effect of alkoxysilanes as external donors in $MgCl_2$-supported Ziegler-Natta catalysts. *Macromolecules* **1992**, *25*, 5914–5918.
11. Sacchi, M.C.; Forlini, F.; Tritto, I.; Locatelli, P.; Morini, G.; Noristi, L.; Albizzati, E. Polymerization stereochemistry with Ziegler-Natta catalysts containing dialkylpropane diethers: a tool for understanding internal/external donor relationships. *Macromolecules* **1996**, *29*, 3341–3345.
12. Noristi, L.; Barbe, P.C.; Baruzzi, G. External donor pair in high-yield catalysts for propylene polymerization, 1. Catalysts-Cocatalyst Interactions. *Makromol. Chem.* **1991**, *192*, 1115–1127.
13. Noristi, L.; Barbe, P.C.; Baruzzi, G. Effect of the internal/external donor pair in high-yield catalysts for propylene polymerization, 2. Polymerization results. *Makromol. Chem.* **1992**, *193*, 229–241.
14. D'Amore, M.; Auriemma, F.; De Rosa, C.; Barone, V. Disordered Chain Conformations of Poly(tetrafluoroethylene) in the High-Temperature Crystalline Form I. *Macromolecules* **2004**, *37*, 9473–9480.
15. Sacchi, M.C.; Forlini, F.; Tritto, I.; Locatelli, P.; Morini, G.; Noristi, L.; Albizzati, E. Polymerization stereochemistry with Ziegler-Natta catalysts containing dialkylpropane diethers: a tool for understanding internal/external donor relationships. *Macromolecules* **1996**, *29*, 3341–3345.
16. Chadwick, J.C.; Van Kessel, G.M.M.; Sudmeijer, O. Regiospecificity and stereospecificity in propene polymerization with $MgCl_2$-supported Ziegler-Natta catalysts - Effects of hydrogen and the external donor. *Macromol. Chem. Phys.* **1995**, *196*, 1431–1437.
17. Chadwick, J.C.; Van Kessel, G.M.M.; Sudmeijer, O. Influence of Ziegler-Natta catalyst regioselectivity on polypropylene molecular weight distribution and rheological and crystallization behavior. *Macromolecules* **2004**, *37*, 9722–9727.
18. Mori, H.; Endo, M.; Terano, M. Deviation of hydrogen response during propene polymerization with various Ziegler-Natta catalysts. *J. Mol.Catal.A* **1999**, *145*, 211.
19. Taniike, T.; Terano, M. Coadsorption and support-mediated interaction of ti species with ethyl benzoate in MgCl2-supported heterogeneous ziegler-natta catalysts studied by density functional calculations. *Macromolecular rapid communications* **2007**, *28*, 1918–1922.
20. Pirinen, S.; Pakkanen, T.T. Polyethers as potential electron donors for Ziegler-Natta ethylene polymerization catalysts. *J. Mol.Catal.A* **2015**, *398*, 177–183.
21. Ratanasak, M.; Rungrotmongkol, T.; Saengsawang, O.; Hannongbua, S.; Parasuk, V. Towards the design of new electron donors for Ziegler-Natta catalyzed propylene polymerization using QSPR modeling. *Polymer* **2015**, *56*, 340–345.
22. Vittoria, A.; Meppelder, A.; Friederichs, N.; Busico, V.; Cipullo, R. Demystifying Ziegler-Natta catalysts: The origin of stereoselectivity. *ACS Catal.* **2017**, *7*, 4509–4518.
23. Cecchin, G.; Morini, G.; Piemontesi, F. *Encyclopedia of Chemical Technology*; Vol. 26, John Wiley and Sons:: New York, (2006); pp. 502–554.
24. Moore, E.P. *Polypropylene Handbook: Polymerization,Characterization, Properties, Applications*; Hanser Publishers:: Munich, Germany, (1996).
25. Chien, J.C.W.; Wu, J.C.; Kuo, C. Magnesium chloride supported high-mileage catalysts for olefin polymerization. IV. FTIR and quantitative analysis of modifiers in the catalysts. *J. Polym. Sci. Polym. Chem. Ed.* **1983**, *21*, 725–736.
26. Chien, J.C.W.; Wu, J.C.; Kuo, C. Coadsorption and support-mediated interaction of ti species with ethyl benzoate in $MgCl_2$-supported heterogeneous ziegler-natta catalysts studied by density functional calculations. *Macromolecular rapid communications* **2007**, *28*, 1918–1922.
27. Stukalov, D.V.; Zakharov, V.A.; Zilberberg, I.L. Adsorption species of ethyl benzoate in MgCl2-supported Ziegler-Natta catalysts. A density functional theory study. *J. Phys. Chem. C* **2010**, *114*, 429–435.
28. Correa, A.; Piemontesi, F.; Morini, G.; Cavallo, L. Key elements in the structure and function relationship of the $MgCl_2$/$TiCl_4$/Lewis base Ziegler-Natta catalytic system. *Macromolecules* **2007**, *40*, 9181–9189.
29. Correa, A.; Credendino, R.; Pater, J.; Morini, G.; Cavallo, L. Theoretical investigation of active sites at the corners of $MgCl_2$ crystallites in supported ziegler-natta catalysts. *Macromolecules* **2015**, *45*, 3695–3701.
30. Credendino, R.; Pater, J.T.M.; Liguori, D.; Morini, G.; Cavallo, L. Investigating alkoxysilane coverage and dynamics on the (104) and (110) surfaces of $MgCl_2$-supported Ziegler-Natta catalysts. *J. Phys. Chem. C* **2012**, *116*, 22980–22986.
31. Credendino, R.; Liguori, D.; Fan, Z.; Morini, G.; Cavallo, L. A Unified Model Explaining Heterogeneous Ziegler-Natta Catalysis. *ACS Catal.* **2015**, *5*, 5431–5435.

32. Capone, F.; Rongo, L.; D'Amore, M.; Budzelaar, P.H.M.; Busico, V. A Periodic Hybrid DFT Approach (Including Dispersion) to $MgCl_2$-supported Ziegler-Natta catalysts 2: Model Electron Donor Adsorption on $MgCl_2$ Crystal Surfaces. *J. Phys. Chem. C* **2013**, *117*, 24345–24353.
33. Seth, M.; Margl, P.M.; Ziegler, T. Polymerization properties of heterogeneous Ziegler-Natta catalyst modified by a base: a theoretical study. *Macromolecules* **2003**, *36*, 6613–6623.
34. Sacchi, M.C.; Forlini, F.; Tritto, I.; Locatelli, P. Stereochemistry of the initiation step in Ziegler-Natta catalysts containing dialkyl propane diethers: a tool for distinguishing the role of internal and external donors. *Macromol. Symp.* **1995**, *89*, 91–100.
35. Rytter, E.; Nirisen, .; Ystenes, M.; Øye, H.A. FTIR Spectroscopy of Ethyl Benzoate-Titanium Tetrachloride Complexes with Application to Supported Ziegler-Natta Catalysts. *Mikrochim.Acta* **1988**, *95*, 85–87.
36. Credendino, R.; Minenkov, Y.; Liguori, D.; Piemontesi, F.; Melchior, A.; Morini, G.; Tolazzi, M.; Cavallo, L. Accurate experimental and theoretical enthalpies of association of TiCl4 with typical Lewis bases used in heterogeneous Ziegler-Natta catalysis. *Phys. Chem. Chem. Phys.* **2017**, *19*, 26996–27006.
37. Terano, M.; Kataoka, T. A study on the states of ethyl benzoate and $TiCl_4$ in $MgCl_2$-supported high-yield catalysts. *Makromol. Chem.* **1987**, *188*, 1477–1487.
38. Corradini, P.; Barone, V.; Fusco, R.; Guerra, G. A possible model of catalytic sites for the stereospecific polymerization of alpha olefins on 1st-generation and supported Ziegler-Natta catalysts. *Gazz.Chim. Ital.* **1983**, *113*, 601.
39. Busico, V.; Cipullo, R. A possible model of catalytic sites for the stereospecific polymerization of alpha olefins on 1st-generation and supported Ziegler-Natta catalysts. *Prog.Polym. Sci.* **2001**, *26*, 443–533.
40. Corradini, P.; Guerra, G.; Cavallo. Do New Century Catalysts Unravel the Mechanism of Stereocontrol of Old Ziegler-Natta catalysts? . *Acc. Chem. Res.* **2004**, *37*, 231–241.
41. Correa, A.; Bahri-Laleh, N.; Cavallo, L. How Well Can DFT Reproduce Key Interactions in Ziegler–Natta Systems? *Macromol. Chem. Phys.* **2013**, *214*, 1980–1989.
42. Wada, T.; Takasao, G.; Piovano, A.; D'Amore, M.; Thakur, A.; Chammingkwan, P.; Bruzzese, P.C.; Terano, M.; Civalleri, B.; Bordiga, S.; et al.. Revisiting the Identity of δ-$MgCl_2$: Part I. Structural Disorder Studied by Synchrotron X-Ray Total Scattering. *J. Catal.* **2020**, *385*, 76–86.
43. Piovano, A.; D'Amore, M.; Wada, T.; Bruzzese, P.C.; Takasao, G.; Thakur, A.; Chammingkwan, P.; Terano, M.; Civalleri, B.; Bordiga, S.; et al.. Revisiting the Identity of δ-$MgCl_2$: Part II. Morphology and Exposed Surfaces Studied by Vibrational Spectroscopies and DFT Calculation. *J. Catal.* **2020**, *387*, 1–11.
44. Corradini, P.; Barone, V.; Fusco, R.; Guerra, G. Analysis of models for the Ziegler-Natta stereospecific polymerization on the basis of non-bonded interactions at the catalytic site—I. The Cossee model. *Eur. Polym. J.* **1979**, *15*, 1133–1141.
45. Boero, M.; Parrinello, M.; Terakura, K. First Principles Molecular Dynamics Study of Ziegler-Natta Heterogeneous Catalysis. *J. Am. Chem. Soc.* **1998**, *120*, 2746–2752.
46. Boero, M.; Parrinello, M.; S. Hüffer, S.; Weiss, H. First Principles Study of Propene Polymerization in Ziegler-Natta Heterogeneous Catalysis. *J. Am. Chem. Soc.* **2000**, *122*, 501–509.
47. Monaco, G.; Toto, M.; Guerra, G.; Cavallo, L. Geometry and stability of titanium chloride species adsorbed on the (100) and (110) cuts of the $MgCl_2$ support of the heterogeneous Ziegler-Natta catalysts. *Macromolecules* **2000**, *33*, 8953–8962.
48. Boero, M.; Parrinello, M.; Weiss, H.; Hüffer, S. A First Principles Exploration of a Variety of Active Surfaces and Catalytic Sites in Ziegler-Natta Heterogeneous Catalysis. *J. Phys. Chem. A* **2001**, *105*, 5096–5105.
49. Seth, M.; Margl, P.M.; Ziegler, T. A Density Functional Embedded Cluster Study of Proposed Active Sites in Heterogeneous Ziegler-Natta Catalysts. *Macromolecules* **2002**, *35*, 7815–7829.
50. Taniike, T.; Terano, M. Reductive Formation of Isospecific Ti Dinuclear Species on a $MgCl_2$ (110) Surface in Heterogeneous Ziegler-Natta Catalysts. *Macromolecular rapid communications* **2008**, *29*, 1472–1476.
51. D'Amore, M.; Credendino, R.; Budzelaar, P.H.M.; Causá, M.; Busico, V. A Periodic Hybrid DFT Approach (Including Dispersion) to $MgCl_2$-supported Ziegler-Natta catalysts 1:$TiCl_4$ Adsorption on $MgCl_2$ Crystal Surfaces. *J. Catal.* **2012**, *286*, 103–110.
52. Breuza, E.; Antinucci, G.; Budzelaar, P.H.M.; Busico, V.; Correa, A.; Ehm, C. $MgCl_2$-supported Ziegler-Natta catalysts: A DFT-D 'flexible-cluster' approach. $TiCl_4$ and probe donor adducts. *Int. J. Quantum Chem.* **2018**, *118*, e25721.
53. Breuza, E.; Antinucci, G.; Budzelaar, P.H.M.; Busico, V.; Correa, A.; Ehm, C. $MgCl_2$-Supported Ziegler–Natta Catalysts: a DFT-D "Flexible-Cluster" Approach to Internal Donor Adducts. *J. Phys. Chem. C* **2018**, *122*, 9046–9053.
54. Credendino, R.; Pater, J.T.M.; Correa, A.; Morini, G.; Cavallo, L. Thermodynamics of Formation of Uncovered and Dimethyl Ether Covered $MgCl_2$ Crystallites. Consequences in the Structure of Ziegler-Natta Heterogeneous Catalysts. *J. Phys. Chem. C* **2011**, *115*, 13322–13328.
55. D'Amore, M.; Thushara, K.; Piovano, A.; Causá, M.; Bordiga, S.; Groppo, E. Surface Investigation and Morphological Analysis of Structurally Disordered $MgCl_2$ and $MgCl_2$/$TiCl_4$ Ziegler-Natta Catalysts. *ACS Catal.* **2016**, *6*, 5786–5796.
56. D'Amore, M.; Piovano, A.; Vottero, E.; Rudic, S.; Groppo, E.; Bordiga, S.; Civalleri, B. Insights on inelastic neutron scattering data of $MgCl_2$ ZN-catalyst support from *ab initio* modelling of nano-sized and disordered models. *ACS Appl. Nano Mater.* **2020**, *3*, 11118–11128.
57. D' Amore, M.; Takasao, G.; Chikuma, H.; Wada, T.; Taniike, T.; Pascale, F.; Ferrari, A.M. Spectroscopic Fingerprints of $MgCl_2$/$TiCl_4$ Nanoclusters Determined by Machine Learning and DFT. *J. Phys. Chem. C* **2021**, *125*, 20048–20058.

58. Thushara, K.; D'Amore, M.; Piovano, A.; Bordiga, S.; Groppo, E. The Influence of Alcohols in Driving the Morphology of Magnesium Chloride Nanocrystals. *ChemCatChem* **2017**, *9*, 1782–1787.
59. Takasao, G.; Wada, T.; Thakur, A.; Chammingkwan, P.; Terano, M.; Taniike, T. Machine Learning-Aided Structure Determination for $TiCl_4$-Capped $MgCl_2$ Nanoplate of Heterogeneous Ziegler-Natta Catalyst. *ACS Catal.* **2019**, *9*, 2599–2609.
60. Takasao, G.; Wada, T.; Thakur, A.; Chammingkwan, P.; Terano, M.; Taniike, T. Insight into Structural Distribution of Heterogeneous Ziegler–Natta Catalyst from Non-empirical Structure Determination. *J. Catal.* **2021**, *394*, 299–306.
61. Piovano, A.; D'Amore, M.; Thushara, K.; Groppo, E. Spectroscopic Evidences for $TiCl_4$/Donor Complexes on the Surfaceof $MgCl_2$-Supported Ziegler-Natta Catalysts. *J. Phys. Chem. C* **2018**, *122*, 5615–5626.
62. Potapov, A.G.; Bukatov, G.D.; Zakharov, V.A. DRIFT study of internal donors in supported Ziegler-Natta catalysts. *J. Mol.Catal.A* **2006**, *246*, 248–254.
63. Potapov, A.G.; Bukatov, G.D.; Zakharov, V.A. DRIFTS study of the interaction of the $AlEt_3$ cocatalyst with the internal donor ethyl benzoate in supported Ziegler-Natta catalysts. *J. Mol.Catal.A* **2009**, *301*, 18–23.
64. Di Noto, V.; Fregonese, D.; Marigo, A.; Bresadola, S. High Yield MgCl2-supported catalysts for propene polymerization: Effects of ethyl propionate as internal donor on the activity and stereospecificity. *Macromol. Chem. Phys.* **1998**, *199*, 633–640.
65. Piovano, A.; Groppo, E. Flexible ligands in heterogeneous catalysts for olefin polymerization: Insights from spectroscopy. *Coordination Chemistry Reviews* **2022**, *451*, 214258.
66. Wada, T.; Funako, T.; Thakur, A.; Matta, A.; Terano, M.; Taniike, T. Structure-performance relationship of $Mg(OEt)_2$-based Ziegler-Natta catalysts. *J. Catal.* **2021**, *389*, 525–532.
67. Taniike, T.; Terano, M. Coadsorption Model for First-Principle Description of Roles of Donors in Heterogeneous Ziegler-Natta Propylene Polymerization. *J. Catal.* **2012**, *293*, 39–50.
68. Hohenberg, P.; Kohn, W. Inhomogeneous Electron Gas. *Phys. Rev.* **1964**, *136*, B864.
69. Kohn, W.; Sham, L.J. Self-Consistent Equations Including Exchange and Correlation Effects. *Phys. Rev.* **1965**, *140*, A1133.
70. Becke, A.D. Density-Functional Thermochemistry. III. The Role of Exact Exchange. *J. Chem. Phys.* **1993**, *98*, 5648–5652.
71. Lee, C.; Yang, W.; Parr, R. Development of the Colle-Salvetti Correlation-Energy Formula Into a Functional of the Electron Density. *Phys. Rev. B* **1988**, *37*, 785–789.
72. Dovesi, R.; Erba, A.; Orlando, R.; Zicovich-Wilson, C.M.; Civalleri, B.; Maschio, L.; Rérat, M.; Casassa, S.; Baima, J.; Salustro, S.; et al.**?**] Quantum-Mechanical Condensed Matter Simulations with CRYSTAL. *WIREs Computational Molecular Science* **2018**, *8*, e1360.
73. Dovesi, R.; Pascale, F.; Civalleri, B.; Doll, K.; Harrison, N.M.; Bush, I.; D'Arco, P.; Noël, Y.; Rérat, M.; Carbonnière, P.; et al.**?**] The CRYSTAL code, 1976–2020 and beyond, a long story. *The Journal of Chemical Physics* **2020**, *152*, 204111. doi:10.1063/5.0004892.
74. Grimme, S. S. Semiempirical GGA-Type Density Functional Constructed with a Long-Range Dispersion Correction. *J. Comput. Chem.* **2006**, *27*, 1787–1799.
75. Grimme, S.; Antony, J.; Ehrlich, S.; Krieg, H. A Consistent and Accurate Ab Initio Parametrization of Density Functional Dispersion Correction (DFT-D) for the 94 Elements H-Pu. *J. Chem. Phys.* **2010**, *132*, 5648–5652.
76. Fornaro, T.; Brucato, J.R.; Feuillie, C.; Sverjensky, D.A.; Hazen, R.M.; Brunetto, R.; D'Amore, M.; Barone, V. Binding of Nucleic Acid Components to the Serpentinite-Hosted Hydrothermal Mineral Brucite. *Astrobiology* **2018**, *18*, 989–1007.
77. Signorile, M.; Vitillo, J.G.; D'Amore, M.; Crocellà, V.; Ricchiardi, G.; Bordiga, S. Characterization and Modeling of Reversible CO_2 Capture from Wet Streams by a MgO/Zeolite Y Nanocomposite. *J. Phys. Chem. C* **2019**, *123*, 17214–17224.
78. Truhlar, D.G. The M06 suite of density functionals for main group thermochemistry, thermochemical kinetics, noncovalent interactions, excited states, and transition elements: two new functionals and systematic testing of four M06-class functionals and 12 other functionals . *Theor. Chem. Acc.* **2008**, *120*, 215–241.
79. Schafer, A.; Horn, H.; Ahlrichs, R. Fully optimized contracted Gaussian basis sets for atoms Li to Kr. *J. Chem. Phys.* **1992**, *97*, 2571–2577.
80. Salustro, S.; Colasuonno, F.; Ferrari, A.M.; D'Amore, M.; Mackrodt, W.C.; Dovesi, R. Substitutional boron and nitrogen pairs in diamond. A quantum mechanical vibrational analysis. *Carbon* **2019**, *146*, 709–716.
81. Platonenko, A.; Gentile, F.S.; Pascal, F.; Ferrari, A.M.; D'Amore, M.; Mackrodt, W.C.; Dovesi, R. Nitrogen substitutional defects in silicon. A quantum mechanical investigation of the structural, electronic and vibrational properties. *Phys. Chem. Chem. Phys.* **2019**, *21*, 20939–20950.
82. Terano, M.; Kataoka, T.; Keii, T. A study on the states of ethyl benzoate and TiCl4 in MgCl2-supported high-yield catalysts. *Die Makromolekulare Chemie* **1987**, *188*, 1477–1487.